Nano Research 2018, 11(8): 4245–4264
https://doi.org/10.1007/s12274-018-2012-1
Research Article
ISSN 1998-0124
CN 11-5974/O4

Stimuli-responsive gel-micelles with flexible modulation of drug release for maximized antitumor efficacy

Djamila Aouameur[1,§], Hao Cheng[1,§], Yaw Opoku-Damoah[1], Bo Sun[2], Qiuling Dong[1], Yue Han[1], Jianping Zhou[1] (✉), and Yang Ding[1] (✉)

[1] *State Key Laboratory of Natural Medicines, Department of Pharmaceutics, China Pharmaceutical University, 24 Tongjiaxiang, Nanjing 210009, China*
[2] *Department of Radiation Oncology, Lineberger Comprehensive Cancer Center, Carolina Center for Cancer Nanotechnology Excellence, Carolina Institute of Nanomedicine, University of North Carolina at Chapel Hill, Chapel Hill, NC 27599, USA*
[§] *Djamila Aouameur and Hao Cheng contributed equally to this work.*

Received: 28 December 2017
Revised: 25 January 2018
Accepted: 26 January 2018

KEYWORDS

stimuli-responsive, cross-linked gel-micelles, biostability, flexible drug release, maximized antitumor efficacy

ABSTRACT

Engineered stimuli-responsive drug delivery devices hold vast promise in biological applications for disease treatment due to their maximized therapeutic efficacy. In this study, a novel, stably cross-linked, and pH-sensitive biodegradable gel-micelle was constructed with amphiphilic conjugates of trimethylene dipiperidine-methacrylic anhydride-hyaluronic acid-stearylamine (TMDP-MA-HA-SA, TMHS) to improve tumor-targeting with flexible intracellular delivery of paclitaxel (PTX). The cross-linked methacrylate bonds significantly improved the biostability of TMHS gel-micelle (~ 200 nm) over the non-cross-linked under physiological conditions, while hyaluronic acid plays an important role in active tumor targetability. The gradual degradation of cross-linked hyaluronic acid shell was triggered by the concentrated hyaluronidase. Meanwhile, under acidic conditions (pH < 6.5), the tertiary amines of pH-sensitive TMDP moieties were protonated and thereby solubilized the gel-micellar core-portions. The resultant pH-triggered inner-core spaces rapidly prompted PTX release in the presence of multiple cytosolic enzymes that mainly degraded the remaining hydrophobic stearylamine core. During the *in vitro* cytotoxicity assay, PTX-loaded TMHS gel-micelles ($^{CL}TMHS_{PTX}$) revealed anticancer efficacy against human hepatocellular carcinoma HepG2 cells with IC_{50} of 1.42 μg/mL (PTX concentration), significantly lower than other groups. In parallel, the *in vivo* anti-tumor efficacy of $^{CL}TMHS_{PTX}$ gel-micelles against BALB/c xenograft tumor animal model demonstrated the greater tumor growth inhibition capacity of 72.06%, compared to other treatment groups at a safe concentration. Consequently, the cross-linked and stimuli-responsive $^{CL}TMHS_{PTX}$ gel-micelles hold a great potential for flexible modulation of intracellular delivery of hydrophobic anticancer drugs with maximized antitumor efficacy.

Address correspondence to Jianping Zhou, zhoujianp60@163.com; Yang Ding, dydszyzf@163.com

1 Introduction

Recently, great efforts have been contributed to design intelligently functionalized nanocarriers for drug delivery in order to efficiently release drugs into tumor tissues in response to variations in physiological environments [1, 2]. The cues include exogenous stimuli, such as temperature alteration [3], magnetic field [4], ultrasonic intensity [5], optical irradiation [6] or electric pulses [7]. Endogenous stimuli include changes in pH [8], enzyme concentration [9] or redox gradients [10]. Moreover, nanosystems responding to multiple stimuli are intended to be effective at assuring extreme drug release under complicated pathological conditions.

Various tumoral matrix-degrading enzymes have been proposed as effective internal stimuli in drug delivery [11, 12]. For instance, hyaluronidase (HAase) is one of the major enzymes in diverse cancers with high concentrations within the tumor microenvironment and tumoral cellular endo/lysosomes, where it is responsible for the catabolism of intracellular hyaluronic acid (HA) within the lysosomes [13]. Therefore, HA-derived conjugates have been extensively applied as HAase-responsive natural polymers for drug delivery, due to their biocompatibility and biodegradability via enzymatic pathways [14]. The polymer is susceptible to cleavage by HAase to yield oligosaccharides and glucuronic acid for drug discharge [15]. Moreover, HA is a tumor-specific ligand and is capable of activating target cluster determinant 44 receptor (CD44) [16], HA receptors (HARE) [17] and HA-mediated motility receptor (RHAMM) [18], which are overexpressed on the surfaces of diverse tumors. Consequently, HA-derived conjugates are an ideal nanocarrier in biomedical applications for targeted drug delivery [19, 20] and tissue engineering [21]. Recent studies confirmed that HA conjugates containing the anticancer agent paclitaxel (PTX) demonstrated enhanced targetability to tumors, amplifying therapeutic efficacy compared to that of free drugs [22]. Inspirationally, the chemical modifications of HA could efficiently alter the material properties and yet maintain its biological characteristics [23]. Various cross-linking strategies, including light and chemical induction processes, have been explored to obtain gel-micelles for micellar biostability [24–26]. These cross-linked gel-micelles based on HA conjugates shared extended duration of cycling in blood and enhanced accumulation in the tumor site [27, 28]. Acidic pH, considered as a typical internal stimulus, has been widely utilized for the responsive release of anticancer agents, as the extracellular tumor pH of 6.5 is lower than the pH 7.4 of major tissues and blood. Moreover, the pH value could be dropped as low as 4.0 to 6.0 in endo/lysosomes [24, 29]. In order to design pH-sensitive micellar constructs, multiple strategies have been utilized to introduce "ionizable" chemical groups into polymeric materials, including amines, carboxylic groups, and phosphate groups, among others. All the groups are amenable to sense slight variations in pH at the tumor-matrix interface and intratumor sub-structures [30, 31]. For instance, 4,4'-trimethylenedipiperidine (TMDP) introduced into an amphiphilic polymer could transform sharply from a hydrophobic to a hydrophilic state via pH-induced protonation [32, 33]. Accordingly, the application of TMDP units for micellar formulation could facilitate stable retention of hydrophobic drugs under the *in vivo* biochemical environment of pH 7.4, and accelerate drug release at lower pH by pH-activated micelle disassembly. To the best of our knowledge, there are few studies on the development of self-assembled hyaluronic gel-micelles inspired from TMDP derivatives to achieve pH-sensitive and intracellular targeted anticarcinogen delivery.

In this study, we have designed stably photo-cross-linked, pH-sensitive, and tumor-targeted gel-micelles based on HA polymers for flexible intracellular delivery of the anticancer drug PTX. The introduction of core-forming materials (stearylamine and TMDP) governs the properties of gel-micelles, including the drug-loading capacity, stability, and controlled drug release profiles. As illustrated in Scheme 1(a), the synthetic amphiphilic conjugates of TMDP-methacrylic anhydride-HA-stearylamine (TMHS) were synthesized using the following steps. To achieve high PTX loading capacity, the hydrophobic stearylamine groups were conjugated with HA polymers to assemble shell-core HA-stearylamine (SA) micelles. Subsequently, the obtained HA-SA conjugates were functionalized with methacrylic anhydride (MA) units, which were able to cross-link and increase the systemic stability of micelles. Finally, the free double-bond ends in copolymers were conjugated with the secondary amine groups of TMDP moieties

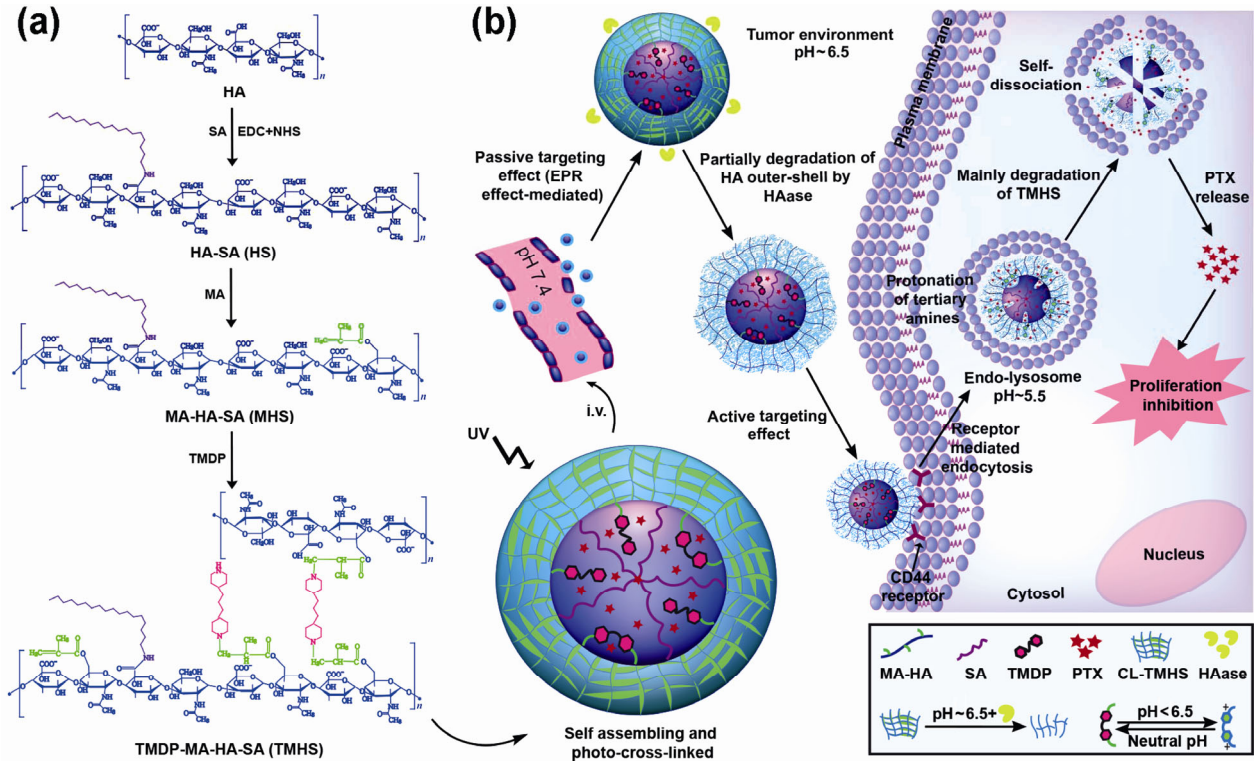

Scheme 1 (a) Schematic design and synthetic procedures of HS, MHS, and TMHS conjugates. (b) Schematic illustration of extracellular and intracellular trafficking pathway of PTX-loaded cross-linked and pH-sensitive TMHS micelles, including accumulation of $^{CL}TMHS_{PTX}$ gel-micelles at the tumor site, gradual degradation of HA gel-shell by HAase at pH ~ 6.5, and receptor-meditated cellular internalization. TMDP moieties became water soluble by pH-sensitive protonation of tertiary amines along with partial disassembly of $^{CL}TMHS_{PTX}$ nanoparticles. The following degradation of $^{CL}TMHS_{PTX}$ nanoparticle inner core by various cytosolic enzymes and endo/lysosomal escape accompanied by burst release of PTX.

to obtain TMHS conjugates containing tertiary amine groups. These groups would protonate and become positively charged and water-soluble below pH 6.5. As depicted in Scheme 1(b), TMHS conjugates were self-assembled into micelles in aqueous solution and formed gel-micelles when triggered by ultraviolet (UV) radiation. After administration, HA outer-shell of gel-micelles could be partially degraded, and the micelles were endocytosed specifically by cancer cells through HA receptor-mediated endocytosis and enhanced permeability and retention effect (EPR). The internalized nanostructure would be further disassembled due to multiple degrading enzymes as well as through pH-induced protonation of tertiary amines, followed by lysosomal membrane disruption and cytoplasmic drug liberation. The antitumor behavior and efficacy of PTX-loaded gel-micelles were investigated both *in vitro* with HepG2 cells and *in vivo* in tumor-bearing mice.

2 Experimental

2.1 Materials

Sodium hyaluronic acid (HA, M_W 23.3 kDa) was purchased from Weifang Lide Bioengineering Co., Ltd. (Shandong, China). SA, MA, 1-ethyl-3-(3-dimethylaminopropyl) carbodiimide (EDC), and N-hydroxysuccinimide (NHS) were purchased from Aladdin Reagent Inc. (Shanghai, China). Paclitaxel was purchased from Shanghai Zhongxi Pharmaceutical (Group) Co., Ltd. (Shanghai, China). TMDP, 3-(4,5-dimethylthiazol-2-yl)-2,5-diphenyl tetrazolium bromide (MTT), coumarin-6 (C6), and Dulbecco's modified Eagle's medium (DMEM), were obtained from Sigma-Aldrich (St. Louis, MO, USA). 1,1′-Dioctadecyl-3,3,3′,3′-tetramethylindotricarbocyanine iodide (DiR) and 4′,6-diamidino-2-phenylindole (DAPI) was obtained from Fanbo Biochemicals Co., Ltd. (Beijing, China). Fetal bovine serum (FBS) and penicillin-streptomycin were obtained from Gibco (USA).

Annexin V-FITC/PI Apoptosis Detection Kit was obtained from Sunshine Biotechnology Co., Ltd. (Jiangsu, China).

2.2 Synthesis and characterization of TMHS copolymer

2.2.1 *Synthesis of stearylamine modified HA (HS)*

Amphiphilic HS conjugates were synthesized through an amination reaction as previously reported with slight modifications [34]. Briefly, 100 mg of HA (M_W 23 kDa) in 5 mL of formamide was blended with EDC (0.5 mM) and NHS (0.5 mM), and the reactants were stirred at ambient temperature for 2 h to activate the carboxyl groups of HA. Next, 0.04 mol of stearylamine in 5 mL of dimethylformamide (DMF) were added dropwise. The reaction solution was maintained with stirring at 60 ˚C for 5 h and then at 25 ˚C for 20 h. The reaction products were firstly refined by precipitation in cold acetone three times, then dialyzed against distilled water, and finally lyophilized to obtain HS conjugates. The chemical constructions of the obtained copolymers were determined by ^{1}H NMR spectra (Avance™ 500, Bruker, Germany) and Fourier transform infrared spectroscopy (FTIR) spectra (Nicolet Avatar™ 370, Thermo, America).

2.2.2 *Synthesis of methacrylic anhydride modified HS (MHS)*

HS conjugates were modified with MA segments to obtain MHS with terminal free double bonds that were able to photo-cross-link with each other. Briefly, 100 mg of HS was completely dissolved in 10 mL of a solution of 50% DMF in H_2O at 4 ˚C under continuous stirring overnight, followed by the addition of MA (3 mol). Continuously stirred, the pH value of the reaction system was adjusted to 8.5 with 0.5 M NaOH. After 24 h of reaction at 4 ˚C, the generated copolymers were firstly purified via precipitation in cold acetone three times, then dialyzed against distilled water [35]. The purified MHS was lyophilized and its chemical structures were detected by ^{1}H NMR spectra and Fourier transform infrared spectroscopy (FTIR) spectra.

2.2.3 *Synthesis of 4,4'-trimethylene dipiperidine anhydride modified MHS (TMHS)*

TMHS conjugates were synthesized via Michael addition of the secondary amine groups of TMDP to the terminal double bonds of the MHS polymer. 100 mg of MHS was dissolved in 10 mL of formamide, and 1 mol of TMDP in 2 mL formamide was added dropwise into the MHS solution. The reactants were stirred at 50 ˚C for 24 h followed by exhaustive dialysis. The solution was filtered through a membrane with 0.8 μm pores, and finally lyophilized. The chemical constructions of the conjugates were characterized by ^{1}H NMR spectra and FTIR spectra.

2.3 Characterizations of TMHS polymer

2.3.1 *Determination of critical micelle concentration (CMC)*

The CMC of TMHS conjugates in de-ionized water was determined through fluorospectrophotometry with use of pyrene as a probe [36]. A series of 10 mL vials were used to contain 1 mL each of pyrene solution (6 mM) in acetone until completely evaporated. TMHS polymers in aqueous solution with serial concentrations ranging from 1×10^{-6} to 2.0 mg/mL were transferred into the bottles. The ultimate pyrene concentration of each sample solution was determined to 6.0×10^{-7} M, and the samples were subsequently sonicated for 30 min. Each sample was incubated at 50 ˚C for 1 h and then left to equilibrate for 12 h at room temperature. Fluorescence spectra of samples was measured by using a fluorescence spectrophotometer (RF-5301 PC; Shimadzu Corp, Kyoto, Japan) at an excitation wavelength of 334 nm and the slit-widths of both excitation and emission were 3 nm. The CMC was estimated as the cross-point when extrapolating the intensity ratio I_{337}/I_{332} at low and high concentration regions.

2.3.2 *Determination of pH sensitivity of TMHS polymer*

To determine pH triggered stability of TMHS conjugates, we have studied the changes of the excitation spectra under different pH values by fluorospectrophotometry with the use of pyrene as a probe. Briefly, 1 mL of pyrene solution (6 mM) in acetone was transferred into the flasks and the solvent was completely evaporated. A total of 10 mL TMHS polymers (41.6 μg/mL) in PBS solutions with pH values varying from 4.5 to 8.5 were also transferred into each corresponding flask with sonication for 30 min. The sample was incubated at 50 ˚C for 1 h, followed by equilibration at ambient temperature for 12 h. The ratios of fluorescence intensities

at 337 and 332 nm (I_{337}/I_{332}) under various pH values were plotted versus pH of the sample solution.

2.4 Preparation and characterization of PTX-loaded MHS and TMHS micelles

2.4.1 *Preparation of drug-loaded micelles*

PTX-encapsulated MHS (MHS_{PTX}) and TMHS ($TMHS_{PTX}$) micelles were manufactured by the dialysis method. Briefly, 15 mg of MHS or TMHS copolymers were dissolved in an aqueous solution of 5 mg/mL. A total of 0.3 mL PTX (10 mg/mL) in methanol was dropped into the conjugate solution and the generated mixture was constantly stirred for 20 min at ambient temperature. Then the system was sonicated for 20 min with a probe-type ultrasonicator (JY 92-2D, Ningbo Scientz Biotechnology Co., Ltd., Nanjing, China) at 100 W. The resulting solution was dialyzed against ultrapure water in a dialysis bag (MWCO 3,500 Da, Solarbio Science & Technology Co., Ltd., Beijing, China) for about 12 h. Finally, the free PTX was removed by micro-pore filtration and the resulting solution was lyophilized.

2.4.2 *UV cross-linking of MHS_{PTX} and $TMHS_{PTX}$ micelles*

The obtained micelles were cross-linked by adding a biocompatible UV initiator, 2-hydroxy-4′-(2-hydroxyethoxy)-2-methylpropiophenone (Irgacure 2959, I2959) to cross-link the micelles. Briefly, I2959 powder was added to MHS_{PTX} or $TMHS_{PTX}$ micelle suspensions, generating a terminal I2959 concentration of 0.1% (w/v). The micellar solution was vortexed for 1 min, and further stirred for 15 min to completely dissolve I2959 powder. The micelle suspension was irradiated for 10 min under UV light to yield cross-linked gel-micelles. The irradiated suspension was then dialyzed for 4 h against distilled water and filtrated through 0.8 μm filter. The blank micelles of MHS and TMHS were cross-linked by the same method described above.

2.4.3 *Characterization of PTX-loaded micelles*

The particle size, polydispersity index (PDI) and zeta potential (ZP) of PTX-loaded micelles were determined by a Dynamic Light Scattering Analyzer (DLS, BI-200SM, Brookhaven Instruments Corp., USA). The morphology of $^{CL}TMHS_{PTX}$ micelles was visualized under transmission electron microscopy (TEM, JEOL JMPEG-PTMC-1230, Japan) operated at 80 kV.

2.4.4 *Drug-loading and encapsulation efficiency determination*

Drug loading (DL) and entrapment efficiency (EE) were determined by high performance liquid chromatography (HPLC, Shimadzu LC-2010 system, Kyoto, Japan). Micelles (0.1 mL) loaded with PTX was diluted with methanol and vortexed for 1 min, and then the samples were centrifuged at 12,000 rpm for 30 min. The supernatant was collected and filtrated through 0.22 μm organic filter, and then 20 μL of filtered solution was subjected to HPLC analysis (Lichrospher™ C18 column, 5 μm particle size, 250 mm × 4.6 mm) to detect PTX concentration at 227 nm wavelength, using 70% methanol aqueous solution as eluant at a flow velocity of 1.0 mL/min. The DL% and EE% were calculated according to Eqs. (1) and (2) as previously reported [37]

$$\mathrm{DL}(\%) = \frac{\text{Weight of PTX in nanoparticles}}{\text{Weight of drug}-\text{loaded nanoparticles}} \times 100\% \quad (1)$$

$$\mathrm{EE}(\%) = \frac{\text{Weight of PTX in nanoparticles}}{\text{Weight of PTX fed initially}} \times 100\% \quad (2)$$

2.5 Stability of non- and cross-linked micelles

In order to investigate the colloidal stability of cross-linked gel-micelles ($^{CL}TMHS_{PTX}$), we have evaluated their stability in serum using non-cross-linked micelles ($^{NCL}TMHS_{PTX}$) as control. Briefly, $^{NCL}TMHS_{PTX}$ and $^{CL}TMHS_{PTX}$ micelles were incubated with 25% (v/v) FBS at 37 °C for 24 h while particle size and PDI were monitored. The storage stability of $^{NCL}TMHS_{PTX}$ and $^{CL}TMHS_{PTX}$ was also studied in PBS solution (pH 7.4) at 4 °C by monitoring changes in particle size and PDI for 6 days.

2.6 *In vitro* drug release from TMHS micelles

In vitro PTX release behaviors of $^{NCL}TMHS_{PTX}$, $^{CL}TMHS_{PTX}$, and $^{CL}TMHS_{PTX}$ + HAase micelles were studied in PBS solutions at pH 4.5, 6.0, and 7.4 using a dialysis method. In brief, 1 mL of each sample containing 0.5 mg/mL of PTX and 0.5 mg/mL of HAase was transferred into a dialysis bag (MWCO 3,500 Da) and submersed in 100 mL of PBS containing 0.1% (w/v) Tween-80 under

shaking at 100 rpm and 37 ˚C. At predesigned time intervals, 2 mL of the release medium was taken and an equal volume of fresh PBS was added. PTX contents were determined by HPLC as described in section 2.4.4.

2.7 Determination of pH sensitivity of PTX-loaded micelles

To confirm pH-sensitive property of TMHS polymeric micelles, we have investigated the changes in particle size and PDI in acidic pH over time. Briefly, 1 mL of micellar suspensions including $^{NCL}MHS_{PTX}$, $^{CL}MHS_{PTX}$, $^{NCL}TMHS_{PTX}$, and $^{CL}TMHS_{PTX}$ were dispersed in PBS buffering solutions at pH 4.5, 6.0, and 7.4, and incubated at 37 ˚C for 24 h. The particle size and PDI were detected at predetermined intervals using DLS.

2.8 Cell culture

For cell studies, human hepatocellular carcinoma HepG2 cells (Shanghai Institute of Biochemistry and Cell Biology, Chinese Academy of Sciences, Shanghai, China) were cultured in DMEM medium supplemented with 10% FBS, 100 U/mL penicillin, and 100 μg/mL streptomycin at 37 ˚C under an atmosphere of 5% CO_2 and 95% relative humidity.

2.9 *In vitro* cellular uptake of TMHS micelles

The intracellular uptake of gel-micelles was investigated with a confocal laser scanning microscopy (CLSM, Leica TCS SP5, Heidelberg, Germany) and flow cytometry (FCM, BD FACS Calibur, USA). The fluorescence marker coumarin-6 (C6) was encapsulated into cross-linked TMHS micelles ($^{CL}TMHS_{C6}$) in the same way as those loaded with PTX. For CLSM analysis, HepG2 cells were seeded on 35 mm culture dishes at a density of 1×10^5 cells/dish and cultured for 24 h. Subsequently, the culture media were exchanged with 1 mL media containing $^{CL}TMHS_{C6}$ gel-micelles at a C6 concentration of 50 ng/mL, and were cultured for 1, 2, and 6 h. At a predesigned timepoint, the medium containing micelles was removed, and the cells were washed and fixed with paraformaldehyde solution (4%, v/v) for 15 min, followed by nuclear staining with DAPI. To investigate whether micelles were specifically internalized by HepG2 cells through endocytosis mediated by HA-receptor, cells were pre-treated with excessive amount of HA (10 mg/mL) for 1 h prior to treatment with $^{CL}TMHS_{C6}$ nanoparticles [38]. Cells without pretreatment were used as a control group, and all samples were observed by CLSM.

For FCM analysis, HepG2 cells were seeded into 24-well plates at a density of 5×10^4 cells/well. Afterwards, 0.5 mL of culture medium containing $^{CL}TMHS_{C6}$ gel-micelles at a C6 concentration of 50 ng/mL was used to culture cells at 37 ˚C. At the same timepoint, the culture media were removed and the cells were washed with cold PBS thrice before resuspension in 0.2 mL of PBS. For competition analysis, cells were pre-incubated with 10 mg/mL HA for 1 h prior to the nanoparticle treatment, and cells without presaturation were used as a control group.

2.10 *In vitro* cytotoxicity assay

The *in vitro* cytotoxicity of blank micelles, PTX-loaded micelles and Taxol® were determined by MTT assay. HepG2 cells were plated in 96-well plate at a density of 1×10^4 cells/well. After cultivation for 24 h, the medium was removed and substituted with 100 μL fresh medium containing PTX-loaded micelles ($^{NCL}MHS_{PTX}$, $^{CL}MHS_{PTX}$, and $^{CL}TMHS_{PTX}$), Taxol® at a range of PTX concentrations (0.001–100 μg/mL), or blank micelles ($^{NCL}MHS_{Blank}$, $^{CL}MHS_{Blank}$, and $^{CL}TMHS_{Blank}$), followed by another 48 h incubation. Thereafter, 20 μL of MTT solution (5 mg/mL) was added to each well and incubated with cells for another 4 h at 37 ˚C. The culture medium was then removed and 100 μL DMSO was added to dissolve the dark blue formazan crystals. The UV absorbance at 570 nm was detected using a microplate reader (EL800, BIO-TEK Instruments Inc., USA). With untreated cells as control, the cell viability (%) was calculated according to Eq. (3)

$$\text{Cell viability (\%)} = \frac{A_{\text{test}}}{A_{\text{control}}} \times 100\% \quad (3)$$

2.11 Cell apoptosis assay

Cell apoptosis was estimated with FACS analysis using the Annexin V-FITC Apoptosis Detection Kit. Briefly, HepG2 cells (2×10^5 cells/well) were seeded in 6-well plates. After cultivation for 24 h, the cells were incubated with samples including Taxol®, $^{NCL}MHS_{PTX}$,

^{CL}MHS$_{PTX}$, and ^{CL}TMHS$_{PTX}$ (PTX concentration was 1.42 μg/mL) using untreated cells as control. After another 24 h of incubation, the cells were resuspended in 100 μL binding buffer and cell apoptosis was detected with FCM according to the manufacturer's protocol.

2.12 Animals and tumor xenograft models

All animal experiments were conducted under a protocol approved by China Pharmaceutical University Ethics Committee and in accordance with the Guide for Care and Use of Laboratory Animals. Tumor-xenografted nude mice were prepared by subcutaneous injection of HepG2 cells (5×10^6 cells per mouse) in the right lateral armpit of BALB/c nude mice (Shanghai Laboratory Animal Center, Shanghai, China). The tumor volume was measured by a caliper and the tumor volume (V) was calculated according to Eq. (4), where L and W represented the length and width of the tumor, respectively.

$$V = L \times W^2 / 2 \quad (4)$$

2.13 *In vivo* fluorescence imaging study

Once tumor volume reached about 200 mm^3, tumor-xenografted nude mice were intravenously administered 200 μL of ^{CL}TMHS$_{DiR}$ DiR-loaded gel-micelles (500 μg/kg of DiR dosage). In the competition group, the tumor-bearing nude mice received high dosage of free HA (50 mg/kg) 1 h ahead of the administration with ^{CL}TMHS$_{DiR}$ to further confirm HA-mediated specific interaction with tumor receptors. At each predetermined interval (1, 4, 8 and 24 h), images were captured with a whole-body optical imaging system (FX PRO, Kodak, USA). After 24 h of live imaging, the animals were sacrificed, and the tumor and primary organs were excised for *ex vivo* imaging. Furthermore, the isolated tumors were embedded in an optimum cutting temperature (OCT) compound, cut into 6 μm sections and stained with DAPI for imaging with CLSM.

2.14 *In vivo* antitumor efficacy

When tumor volume reached approximately 100 mm^3, the mice were randomized into 5 groups (n = 5) and administered ^{NCL}MHS$_{PTX}$, ^{CL}MHS$_{PTX}$, ^{CL}TMHS$_{PTX}$, Taxol®, and saline at a PTX dose of 10 mg/kg, respectively. The mice were injected via tail vein once every 2 days for 11 days. Tumor volumes and body weights were recorded after each administration. Mice were sacrificed at day 12 after termination of treatment and the tumors were excised and weighed. Tumors and primary organs were also harvested for histological examination with hematoxylin and eosin (H&E) staining.

2.15 Safety profiles

Hemolysis studies were conducted to estimate the safety of TMHS micelles for intravenous injection. Red blood cells (RBC) were collected from New Zealand rabbit and diluted with normal saline to obtain a terminal concentration of 2%. ^{CL}TMHS$_{PTX}$ and Taxol® were diluted with saline to different PTX concentrations (0.01–0.2 mg/mL), while ^{CL}TMHS$_{Blank}$ and Cremophor EL and ethanol (1/1, v/v) were diluted to different carrier concentrations (0.08–1.6 mg/mL). Subsequently, 2% RBC suspensions were incubated with tested samples of the same volume at 37 ˚C for 1 h followed by centrifugation at 3,000 rpm for 10 min. The absorbance of the supernatants was measured with microplate reader at 540 nm. Zero hemolysis or 100% hemolysis were obtained from red blood cells suspended in normal saline or distilled water, respectively. The percentage of hemolysis was determined according to following Eq. (5)

$$\text{Hemolysis}\ (\%) = \frac{A_{\text{sample}} - A_{0\%}}{A_{100\%} - A_{0\%}} \times 100\% \quad (5)$$

For adverse effect assessment *in vivo*, 15 healthy BALB/c mice (6–7 weeks old) were randomly divided into 3 groups (n = 5). Saline, Taxol® (10 mg/kg of PTX), and ^{CL}TMHS$_{PTX}$ (10 mg/kg of PTX) were injected intravenously every 2 days for 11 days. Blood was collected on Day 13 to evaluate liver functions, including alanine amino transferase (ALT) and alkaline phosphatase (ALP), and renal functions, including blood urea nitrogen (BUN) and creatinine (CRE). The mice were then sacrificed and the primary organs including heart, liver, spleen, lung, and kidney were collected for H&E staining.

2.16 Statistical analysis

Data were presented as means ± standard deviation (SD) from at least triplicate experiments performed in a parallel manner unless otherwise indicated. Statistical

significance was tested using one-way or two-way ANOVA, and significance of difference was indicated as $*p < 0.05$, $**p < 0.01$, and $***p < 0.001$.

3 Results and discussion

3.1 Synthesis and characterization of polymers

Herein, a cross-linkable, pH-sensitive, and biodegradable copolymer TMHS was synthesized following the procedures exhibited in Scheme 1(a). Initially, the hydrophilic polymer HA was functionalized with hydrophobic SA to obtain amphipathic structure HS. Subsequently, the HS copolymer was conjugated with MA groups to yield cross-linkable MHS, which was further modified with the hydrophobic amine donor TMDP via Michael addition to endow TMHS conjugates with pH-sensitivity. The obtained conjugates of each synthesis-step were characterized and verified by ^{1}H NMR and FTIR. As shown in ^{1}H NMR spectra (Fig. 1(a)), the new peaks of HS conjugates at 0.90, 1.20–1.35, and 2.98 ppm were assigned to the alkyl groups of the long-chain stearylamine group compared with that of HA spectrum. For MHS conjugates, the characteristic peaks of MA protons appeared at 1.90, 5.78, and 6.20 ppm attributable to MA's methyl protons and the methacrylate protons, respectively. The TMHS spectrum demonstrated new characteristic peaks of TMDP and amino-ester segments at 1.00–1.20, 1.40, 1.65, 2.65, 2.75, and 3.05 ppm. In addition, compared to the FTIR spectrum of HA (Fig. 1(b)), the new amide I (C=O of acylamide) and amide II (C–N of acylamide) bands in HS conjugates appeared at 1,652.6 and 1,563.5 cm^{-1}. The main absorption band of MHS conjugates at 1,739.0 cm^{-1} attributed to the carbonyl stretching (C=O) of the newly generated ester band.

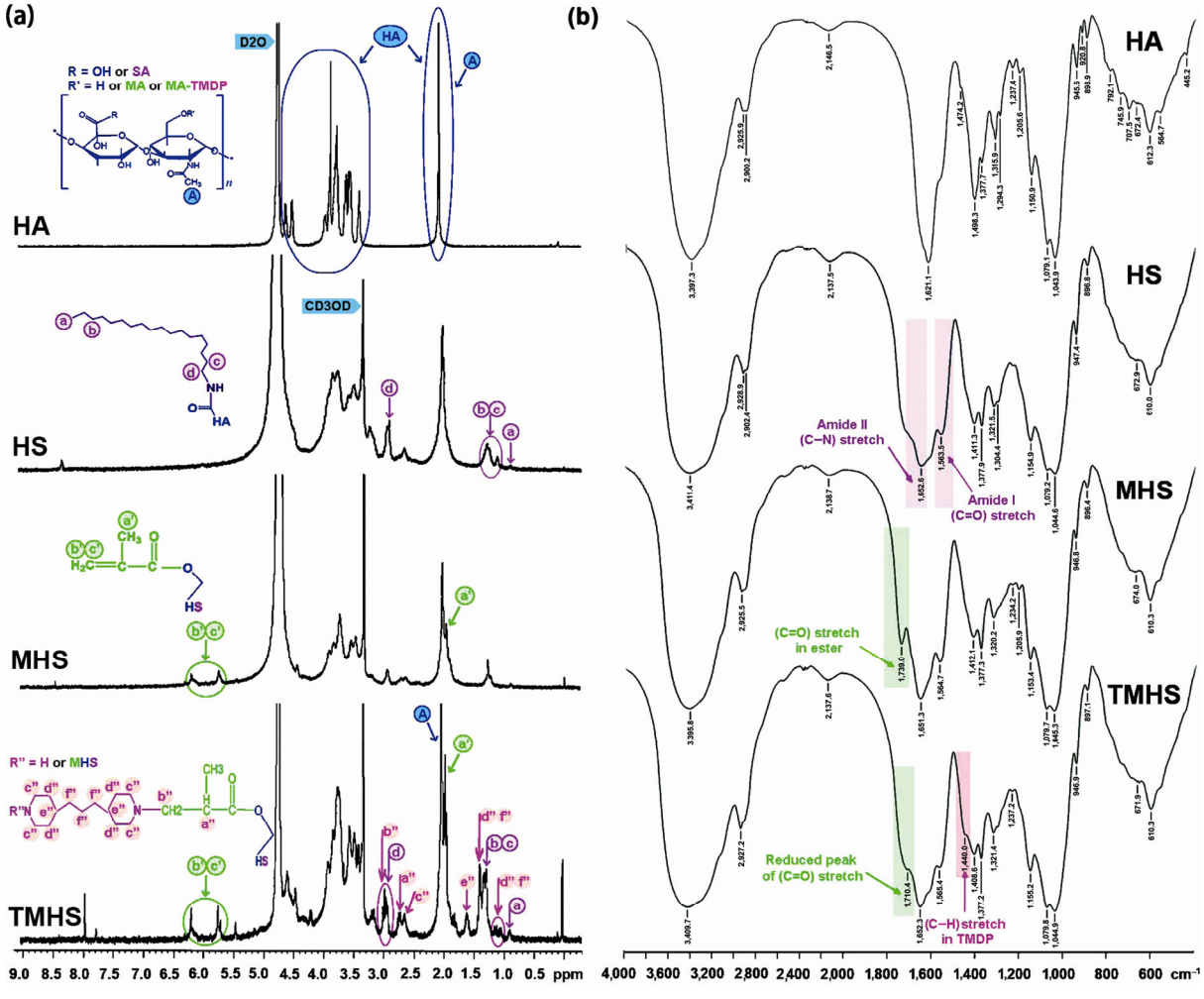

Figure 1 ^{1}H NMR spectra (a) and FTIR spectra (b) of various modified polymer conjugates.

Compared to the spectrum of MHS, the spectrum of TMHS displayed a burst decrease in the stretch of the ester carbonyl peak at 1,710.4 cm^{-1} due to the conjugation of the terminal double bonds with amine groups of TMDP moieties. A small peak also appeared at 1,440.0 cm^{-1} assigned to the methylenes of TMDP, further confirming successful synthesis of TMHS, and MHS used as control copolymer. The degrees of substitution of SA, MA, and TMDP to HA were 3.8%, 24.3%, and 7.4%, respectively.

3.2 Characterizations of TMHS polymer

To evaluate the capability of TMHS polymers for stable polymeric micelle formulation and their aggregation behavior in aqueous medium, the CMC was determined by fluorescence spectroscopy using pyrene as a probe. The results revealed that TMHS shared a low CMC value of 4.16 μg/mL, which we attributed to high hydrophobicity induced by SA lipid and TMDP segments, reducing the polymer micelle fluidity for superior micellization functions. The low CMC value would ensure the stability of micelles during blood circulation, thereby avoiding drug release prior to reaching the targeting site. The pH sensitivity of TMHS conjugates was evaluated by DLS with pyrene as a probe (Fig. 2(a)). When the pH value of the conjugate solution exceeded 7, the ratio of I_{337}/I_{332} showed little variation, demonstrating a stabilized core-shell structure; and while the pH value switched from 7 to 6.5, there was a sharp reduction of I_{337}/I_{332} ratio. This transition with respect to pH was in accordance with the natural properties of these groups. The tertiary amines of TMDP hydrophobic groups in TMHS copolymer become protonated and water-soluble in an acidic environment. The I_{337}/I_{332} ratio maintained a low and stable value at pH < 6.5 owing to the further protonation of tertiary amines and consequent dissolution of TMHS conjugates. Based on these results, TMHS micelles provided with such a low transition pH range could remain stable in the extracellular space and subsequently be internalized into the cytosol to achieve flexible modulation of intracellular drug release.

3.3 Preparation and characterization of PTX-loaded polymeric micelles

A series of MHS and TMHS micellar formulations were constructed by the dialysis method followed by UV-mediated cross-linking, and micelles without crosslinking were prepared as a control. Figure 2(b) showed gel formation of the TMHS polymer after exposure to UV-irradiation in the presence of I2959 as a photo-initiator. This indicates photo cross-linking of terminal double bonds of TMHS conjugates. The MHS and TMHS micelles are characterized by primary physicochemical parameters including particle size, PDI, DL%, and EE% (Table 1). As demonstrated, the particle diameter of $^{CL}TMHS_{PTX}$ gel-micelles decreased approximately 20 nm compared to that of $^{NCL}TMHS_{PTX}$, and the similar reduction in diameter was observed for $^{CL}MHS_{PTX}$ and $^{NCL}MHS_{PTX}$. In accordance with diameter, the PDI of PTX-loaded TMHS or MHS micelles can also be reduced by cross-linking of the HA corona. Accordingly, $^{CL}TMHS_{PTX}$ gel-micelles demonstrated the lowest PDI of 0.173 indicating a narrow size distribution (Fig. 2(c)). Both the EE% and DL% of $^{CL}TMHS_{PTX}$ were higher than those of $^{NCL}MHS_{PTX}$ and $^{CL}MHS_{PTX}$, which we attributed to the increased hydrophobic interactions between PTX and the micellar core after the introduction of TMDP. In addition, negative surface charges of −30 mV were confirmed in series of polymeric micelles, which we attributed to the remaining carboxyl groups of HA corona. Furthermore, TEM image (Fig. 2(d)) exhibited well-distributed spheres of $^{CL}TMHS_{PTX}$ gel-micelles.

3.4 The effects of cross-linking on the stability of PTX-loaded TMHS micelles

For tumor-specific drug delivery and the reduction of systemic side effects, the compact structure of nanoparticles should have high stability in the *in vivo* milieu to avoid cargo leakage prior to arrival at tumor site. To investigate the structural integrity of PTX-loaded TMHS micelles under physiologically relevant conditions, we monitored the changes in diameter and PDI of $^{NCL}TMHS_{PTX}$ and $^{CL}TMHS_{PTX}$ in the presence of 25% FBS against time intervals using DLS (Fig. 2(e)). $^{CL}TMHS_{PTX}$ gel-micelles demonstrated negligible variation in particle size (< 10%) and PDI (< 6%) within 24 h of incubation, while $^{NCL}TMHS_{PTX}$ showed dramatic changes in both particle size (50.9%) and PDI (55.14%). These results indicated that the close-knit cross-linked HA corona imbued the TMHS micelles with high structural integration by protecting the micelles and payloads from protein interaction or ion displacement. Moreover,

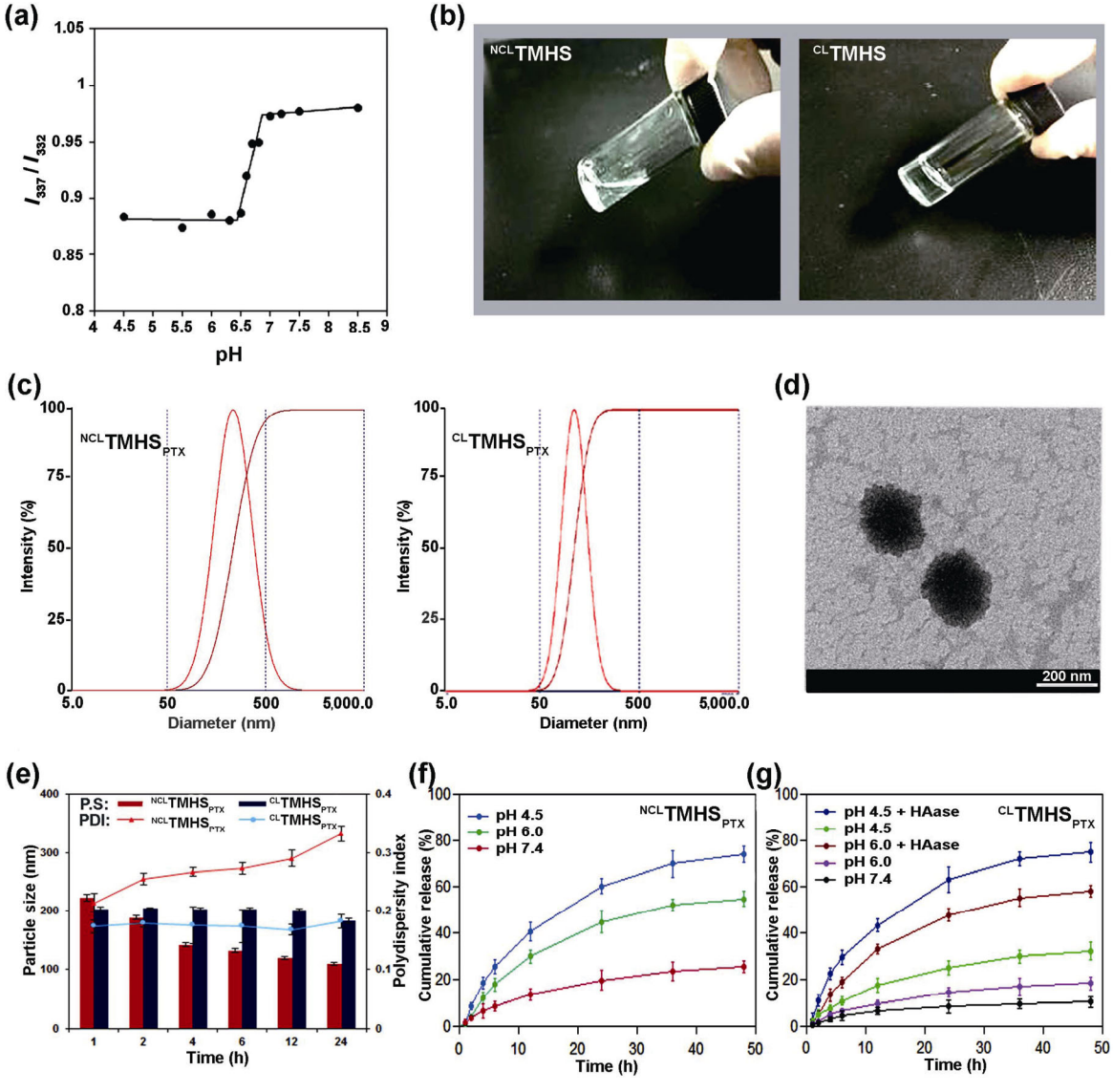

Figure 2 (a) Variations of the intensity ratio (I_{337}/I_{332}) in pyrene loaded TMHS micelles in a variety of pH values determined by fluorospectrophotometry. (b) Hydrogel formation of TMHS conjugates via UV irradiation in the presence of I2959 in contrast to non-cross-linked TMHS conjugates. (c) The hydrodynamic particle size distribution of $^{CL}TMHS_{PTX}$ and $^{NCL}TMHS_{PTX}$ nanoparticles measured by DLS. (d) TEM image of $^{CL}TMHS_{PTX}$ gel-micelles. (e) Stability study of $^{NCL}TMHS_{PTX}$ and $^{CL}TMHS_{PTX}$ nanoparticles upon incubation with FBS (25%, v/v) by monitoring particle size and PDI changes within 24 h of incubation. *In vitro* release behavior of PTX from $^{NCL}TMHS_{PTX}$ micelles (f) and $^{CL}TMHS_{PTX}$ gel-micelles (g) in the presence or absence of HAase at different pH. Data are presented as mean ± SD, $n = 3$.

Table 1 Characteristics of series of PTX-loaded micelles. Data are presented as mean ± SD, $n = 3$. *$p < 0.05$, **$p < 0.01$, and ***$p < 0.001$

Samples	Size (nm)	PDI	DL (%)	EE (%)
$^{NCL}MHS_{PTX}$	243.17 ± 4.37***	0.24 ± 0.023**	11.40 ± 0.50**	56.97 ± 2.49**
$^{CL}MHS_{PTX}$	224.60 ± 4.67**	0.22 ± 0.016*	11.01 ± 0.23**	55.03 ± 1.17**
$^{NCL}TMHS_{PTX}$	222.79 ± 5.63**	0.21 ± 0.015*	13.26 ± 0.47	66.28 ± 2.35
$^{CL}TMHS_{PTX}$	202.36 ± 4.73	0.17 ± 0.011	12.67 ± 0.06	63.35 ± 0.28

^{CL}TMHS$_{PTX}$ gel-micelles displayed desirable storage stability in PBS buffer at 4 ℃ compared to that of ^{NCL}TMHS$_{PTX}$ micelles (Fig. S2 in the Electronic Supplementary Material (ESM)). The average particle size and PDI of ^{CL}TMHS$_{PTX}$ gel-micelles were almost constant within 6 days of storage, approximately around 200 nm and 0.17, respectively. In contrast, significant changes in particle diameter and PDI of ^{NCL}TMHS$_{PTX}$ micelles were monitored within the same storage period. All results above provided substantial evidence that cross-linking greatly enhanced the biostability of TMHS micelles.

3.5 *In vitro* PTX release profile

The terminal purpose of cross-linked TMHS gel-micelles is for intracellular delivery and stimuli-responsive release of drug PTX. To confirm that the enhanced drug release from TMHS micelles was triggered by cellular stimuli, such as acidic pH and HAase, the cumulative release profile of PTX was observed using a dialysis bag in different buffering media (Figs. 2(f) and 2(g)). The cumulative PTX release from ^{CL}TMHS$_{PTX}$ gel-micelles at pH 7.4 was 25.50% in 48 h, whereas that released from ^{NCL}TMHS$_{PTX}$ micelles dramatically increased to 54.70% and 73.97% by decreasing pH to 6 and 4.5, respectively. The comparative drug release profile revealed that ^{NCL}TMHS$_{PTX}$ micelles could release drug in a pH-dependent manner with greater release rates at lower pH values. This was attributed to the improved hydrophilicity of protonated TMHS, thereby increasing the dissociation between TMHS nanoparticles and payload PTX. At all pH conditions tested, PTX release from ^{CL}TMHS$_{PTX}$ gel-micelles was notably slower than that from ^{NCL}TMHS$_{PTX}$ micelles, indicating the sustained drug release pattern and the desirable biostability of ^{CL}TMHS$_{PTX}$ gel-micelles in the blood stream. Furthermore, when HAase was introduced into buffer solutions at pH 6.0 or pH 4.5, the PTX release rate was notably accelerated, when compared with that in corresponding medium without HAase. After incubation with HAase at pH 6.5 and 4.5, 57.80% and 74.88% of PTX, respectively, were released from ^{CL}TMHS$_{PTX}$ gel-micelles within 48 h. In contrast, only 18.25% (pH 6.5) and 32.24% (pH 4.5) of PTX were released from ^{CL}TMHS$_{PTX}$ nanoparticles in the absence of HAase within 48 h. Furthermore, the percentages of released PTX from ^{CL}TMHS$_{PTX}$ in the presence of HAase at pH 6 and 4.5 were almost the same as that from ^{NCL}TMHS$_{PTX}$ at the same acidic pH. The above results indicated that HAase was effective in the initiation of PTX release from ^{CL}TMHS$_{PTX}$ by the gradual degradation of ^{CL}TMHS$_{PTX}$ outer close-knit HA corona, leading to burst PTX release from ^{CL}TMHS$_{PTX}$ in acidic pH medium.

3.6 The pH-dependent characteristics of PTX-loaded TMHS micelles

The pH sensitivity of PTX-loaded TMHS micelles with or without cross-linking were investigated by monitoring the changes in particle size and PDI using DLS in response to increasingly acidic media (pH 7.4, 6.0, and 4.5) over 24 h (Fig. 3(a)). The particle size and PDI of ^{NCL}TMHS$_{PTX}$ micelles greatly increased, accompanied by a decrease in pH. After 24 h of ^{NCL}TMHS$_{PTX}$ micelle incubation in different media, we recorded particle diameters which increased from 222.79 to 433.67 nm (pH 6.0) and 523.8 nm (pH 4.5), and PDI from 0.214 to 0.293 (pH 6.0) and 0.341 (pH 4.5), respectively. The ^{CL}TMHS$_{PTX}$ micelles had stable particle size and PDI within the first 4 h of incubation in acidic conditions, followed by a moderate increase in both particle size and PDI (Fig. 3(b)). For comparison, ^{CL}TMHS$_{PTX}$ gel-micelles underwent size increases from 202.36 to 247.30 nm (pH 6.0) and 255.33 nm (pH 4.5), and PDI from 0.173 to 0.211 (pH 6.0) and 0.245 (pH 4.5) after 24 h incubation. Moreover, ^{CL}TMHS$_{PTX}$ gel-micelles shared higher structural stability at pH 7.4 as compared with ^{NCL}TMHS$_{PTX}$ micelles that displayed a remarkable size increase at 24 h. These changes in size and PDI at pH ≤ 6 indicated that drug-loaded micelles of ^{NCL}TMHS$_{PTX}$ and ^{CL}TMHS$_{PTX}$ nanoparticles simultaneously demonstrated pH-dependent swelling and disassembly. This resulted from the protonation of TMDP tertiary amine groups in the micellar core that were partially converted to a water-soluble form. The gel-micelles of ^{CL}TMHS$_{PTX}$ maintained the core-shell micellar structure attributed to the covalent cross-linked HA corona; and the HA outer-shell was intended to be cleavable by concentrated HAase in the tumor environment. For further confirmation, we have detected the changes in size and PDI of the non-pH-sensitive MHS nanoparticles including ^{NCL}MHS$_{PTX}$ and ^{CL}MHS$_{PTX}$ (Figs. 3(c) and 3(d)). Drug-loaded MHS micelles revealed almost no variation in particle size and PDI by increasing the acidity within the incubation time. However, the particle size of ^{NCL}MHS$_{PTX}$ at 24 h

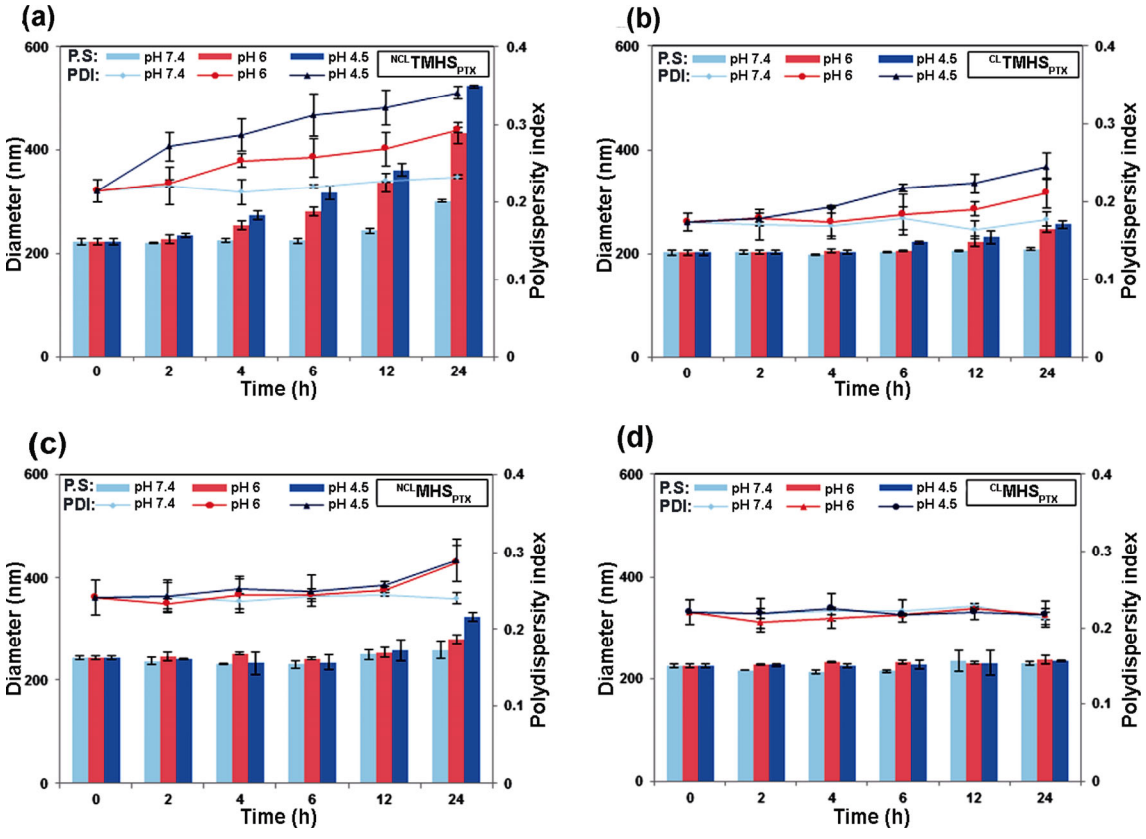

Figure 3 The pH-dependent behavioral changes in particle size and PDI of $^{NCL}TMHS_{PTX}$ (a), $^{CL}TMHS_{PTX}$ (b), $^{NCL}MHS_{PTX}$ (c), and $^{CL}MHS_{PTX}$ (d) micelles under various pH conditions. Data are expressed as mean ± SD, $n = 3$.

increased by around 37 nm (pH 6.0) and 80 nm (pH 4.6), which was likely due to the hydrolysis of the amide bonds of SA conjugated with carboxylic groups of HA under acidic conditions [39]. The above results indicated highly pH-sensitive structural stability of TMHS micelles compared to that of MHS micelles, owing to the existence of pH-sensitive TMDP units within the inner-core. The UV initiated cross-linking strategy moderated the speed of pH-triggered degradation in TMHS gel-micelles.

3.7 *In vitro* cellular internalization

HA receptors, such as CD44 and RHAMM, have been demonstrated to be highly expressed on the cytomembrane of various malignant neoplasms, which has given rise to extensive research on HA-derived copolymers in tumor-targeted drug delivery. To validate TMHS-mediated intracellular delivery of PTX, we have studied the cellular uptake of C6-loaded TMHS gel-micelles ($^{CL}TMHS_{C6}$) and the intracellular release of the encapsulated payload within HepG2 cells by CLSM. The $^{CL}TMHS_{C6}$ group revealed bright green fluorescence signals in the cytoplasm of HepG2 cells (Fig. 4(a)), indicating sufficient intake of $^{CL}TMHS_{C6}$ by HepG2 cells. In addition, the fluorescence intensity of C6 gradually increased during the 1 to 6 h incubation, suggesting that the cellular nanoparticle internalization increased in a time-dependent manner. To further illustrate the internalization mechanism of TMHS gel-micelles, a competition experiment was conducted by incubating HepG2 cells with an excess of HA for 1 h prior to treatment with TMHS gel-micelles. As expected, the fluorescence intensity of the $^{CL}TMHS_{C6}$ group decreased significantly after pre-treatment with free HA, confirming that TMHS gel-micelles were endocytosed by cells via HA receptor-mediated endocytosis. The intracellular internalization of $^{CL}TMHS_{C6}$ was quantitatively analyzed by FCM (Figs. 4(b) and 4(c)). After incubation for 6 h, C6 signal intensity of $^{CL}TMHS_{C6}$ was approximately 1.6-fold higher than that of $^{CL}TMHS_{C6}$ pretreated with free-HA, further indicating the role of HA receptors in the internalization of TMHS gel-micelles.

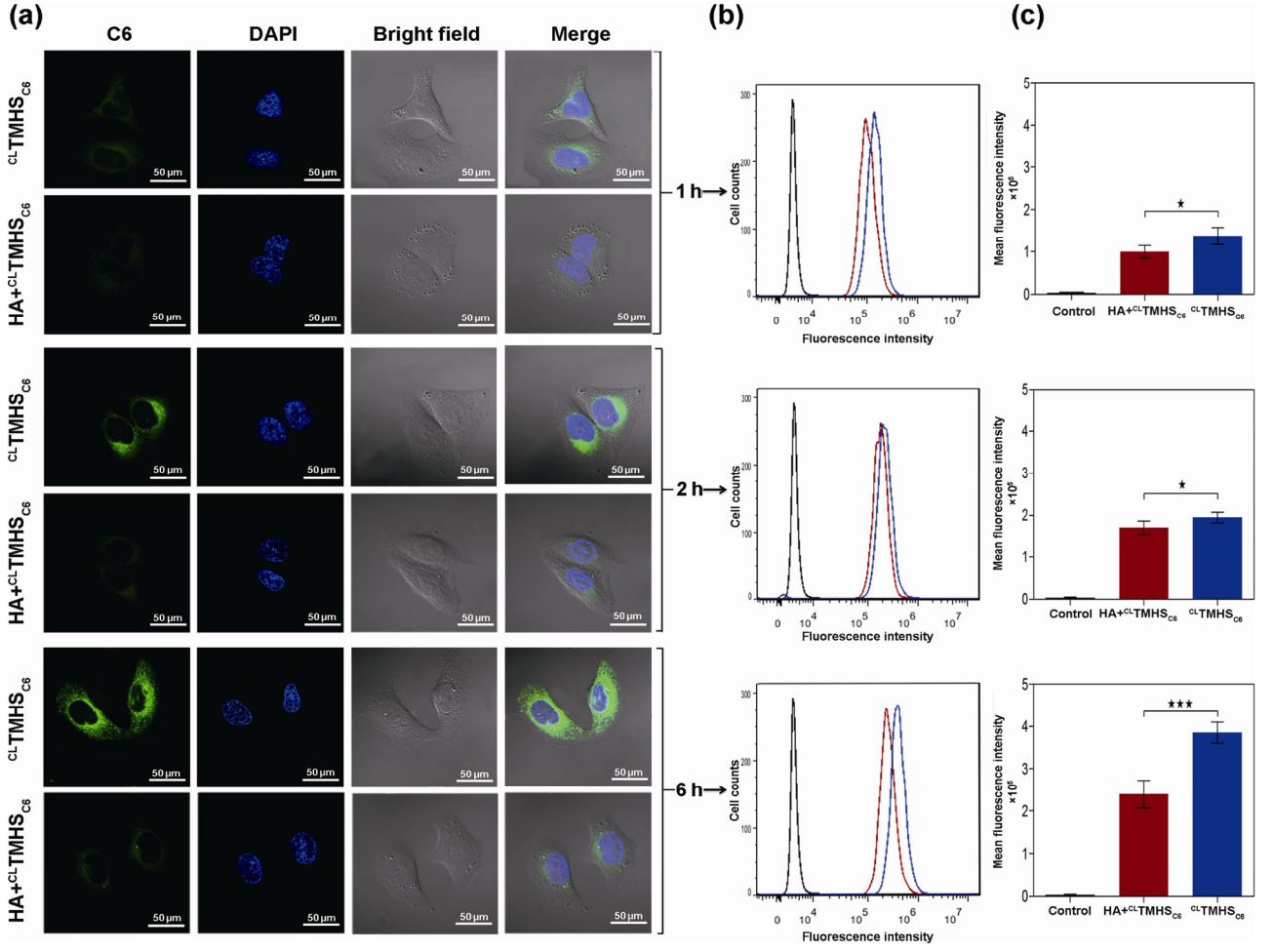

Figure 4 (a) Cellular uptake of ^{CL}TMHS$_{C6}$ with and without free HA preincubation in HepG2 cells during predetermined incubation time (1, 2 and 6 h) by CLSM. Nuclei were stained using DAPI (blue color), and scale bar is 50 μm. Representative FACS images (b) and quantitative flow cytometric analysis (c) of intracellular internalization of ^{CL}TMHS$_{C6}$ with and without HA preincubation in HepG2 cells at 1, 2 and 6 h. Data are expressed as mean ± SD, n = 3.

3.8 *In vitro* antitumor efficacy

The *in vitro* cytotoxicity of blank micelles (^{NCL}MHS$_{Blank}$, ^{CL}MHS$_{Blank}$ and ^{CL}TMHS$_{Blank}$) and PTX preparations (^{NCL}MHS$_{PTX}$, ^{CL}MHS$_{PTX}$, ^{CL}TMHS$_{PTX}$, and Taxol®) against HepG2 cells was estimated by MTT assay. As shown in Fig. 5(a), cell viability of various blank micelle groups was approximately 100% even at the maximum test concentration (500 μg/mL). The results suggested that the functionalized conjugates and corresponding micelles had negligible cytotoxicity to HepG2 cells and were safe to be used as a drug carrier. All PTX preparations of ^{NCL}MHS$_{PTX}$, ^{CL}MHS$_{PTX}$, ^{CL}TMHS$_{PTX}$, and Taxol® revealed PTX dose-dependent cytotoxicity against HepG2 cells (Fig. 5(b)). In particular, ^{CL}TMHS$_{PTX}$, demonstrated a significantly greater cytotoxicity in comparison to that of ^{CL}MHS$_{PTX}$ and ^{NCL}MHS$_{PTX}$ at a PTX-dose ≥ 0.01 μg/mL. Furthermore, Table 2 lists the half-maximal inhibitory concentration (IC_{50}) of the tested preparations. ^{CL}TMHS$_{PTX}$ displayed a notably lower IC_{50} of 1.42 μg/mL, confirming that CD44 receptor-mediated endocytosis, followed by the PTX release triggered by acidic pH and HAase enhanced the cytotoxicity of PTX gel-micelles. Interestingly, ^{CL}TMHS$_{PTX}$ micelles presented a higher cytotoxicity than Taxol® at a PTX-dose ≤ 10 μg/mL; whereas at PTX-dose ≥ 75 μg/mL, Taxol® exhibited sharp increase in cell killing activity, even higher than ^{CL}TMHS$_{PTX}$ group, remarkably. The findings could be attributed to the existence of Cremophor EL in Taxol® which was reported to cause obvious inhibition of cell activity at high concentrations [40]. Moreover, micromolecular free drugs such as PTX in Taxol® can be passively transported into cells due to their high concentration

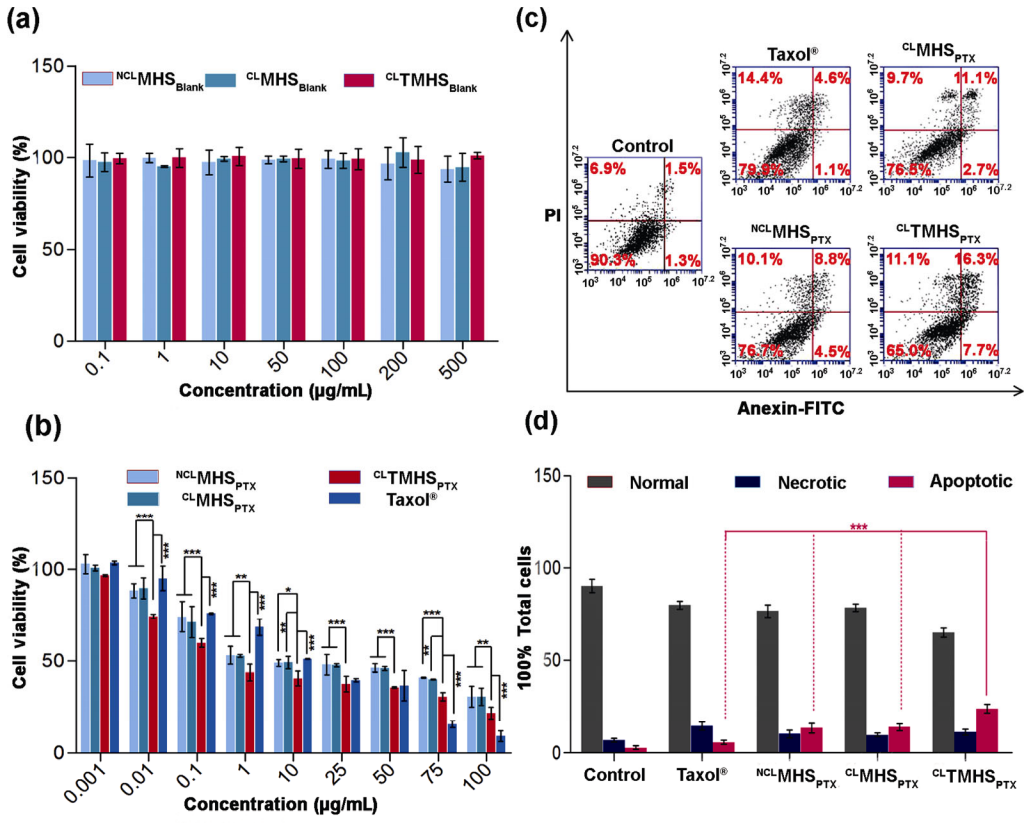

Figure 5 *In vitro* cytotoxicity of blank micelles (a) and PTX preparations (b) against HepG2 cells with different concentrations for 48 h. Representative images (c) and flow cytometric analysis (d) of HepG2 cell apoptosis induced by various PTX preparations at 24 h. Data are expressed as mean ± SD, $n = 5$, $^{*}p < 0.05$, $^{**}p < 0.01$, and $^{***}p < 0.001$.

Table 2 Inhibitory concentration (IC_{50}) of different PTX preparations in HepG2 cells for 48 h. Data are expressed as mean ± SD, $n = 5$, $^{***}p < 0.001$ vs. other groups

Formulations	Taxol®	$^{NCL}MHS_{PTX}$	$^{CL}MHS_{PTX}$	$^{CL}TMHS_{PTX}$
IC_{50} (μg/mL)	5.72	10.18	9.38	1.42***

in the *in vitro* environment [40, 41]. Even in the highest concentration (100 μg/mL) the PTX would not precipitate in cell culture medium. However, macromolecular assemblies like TMHS micelles and MHS micelles need to be pre-internalized via a time-dependent endocytosis pathway. The payloads were further released after a delay due to cytosolic and endonuclear shuttling. Consequently, the anti-proliferative effects of Taxol® were greatly enhanced *in vitro* at high concentrations. These findings together revealed that the functionalized conjugates were safe for drug delivery. The pH-sensitive release and CD44 receptor-mediated endocytosis played an important role in the increased cytotoxicity of TMHS micelles.

According to the design of $^{CL}TMHS_{PTX}$-modulated flexible PTX delivery and release, the *in vitro* therapeutic efficacy of $^{CL}TMHS_{PTX}$ gel-micelles was verified through the Annexin V-FITC/PI (propidium iodide) double labeling assay (Figs. 5(c) and 5(d)). After 24 h of incubation, the $^{CL}TMHS_{PTX}$ group induced the most significant apoptosis rate of 24.0%, compared to other PTX preparations (5.7% for Taxol®, 13.3% for $^{NCL}MHS_{PTX}$ and 13.8% for $^{CL}MHS_{PTX}$). The findings corresponded to the results observed in cytotoxicity and suggested that acid-activation of $^{CL}TMHS_{PTX}$ gel-micelles greatly accelerated intracellular PTX release for maximal apoptosis activity.

3.9 *In vivo* imaging for targeting analysis

The majority of previously reported nano-sized drug delivery systems have revealed insufficient target ability *in vivo* due to clearance of nanoparticles from blood stream and deficiency of internalization by

tumor cells. Hence, a cross-linked HA corona was used in $^{CL}TMHS_{PTX}$ for prolonged circulation persistence and increased tumor-site accumulation due to the detachable outer shell and receptor-mediated endocytosis. To investigate the *in vivo* tumor-targeting efficiency of TMHS nanoparticles, $^{CL}TMHS_{DiR}$ gel-micelles were administrated into HepG2 tumor xenograft nude mice via tail vein injection. Subsequently, *in vivo* biodistribution was monitored at 1, 4, 8, and 24 h post-injection within a whole-body fluorescence imaging system (Fig. 6(a)). The $^{CL}TMHS_{DiR}$ group revealed a noteworthy fluorescence signal at the tumor site after 1 h injection. At the later time intervals the fluorescence signal continued strengthening gradually and reached a maximum value at 8 h post-injection, suggesting an efficient tumor targeting ability of TMHS gel-micelles. In addition, a long-lasting fluorescence signal was distinctly observed at the tumor site of $^{CL}TMHS_{DiR}$ group even 24 h post-injection, confirming enhanced retention within tumors of the cross-linked TMHS carriers. To further confirm the targeting efficiency of the HA corona towards cancer cells expressing high levels of CD44 receptor, a high dose of free HA was administrated prior to injection of $^{CL}TMHS_{DiR}$ to saturate CD44 receptors on HepG2 cells. The appearance of fluorescent signal was markedly delayed as expected, and almost no accumulation was observed at 1 h post injection. Furthermore, obvious attenuation of DiR fluorescence signal at tumor site was visualized at every time point and compared to that of the non-pretreatment group. The results revealed that a close-knit HA corona could promote tumor accumulation of TMHS gel-micelles via active targeting pattern.

At 24 h post-injection, the tumors and main organs were excised after euthanasia for *ex vivo* imaging. According to quantitative region-of-interest (ROI) analysis,

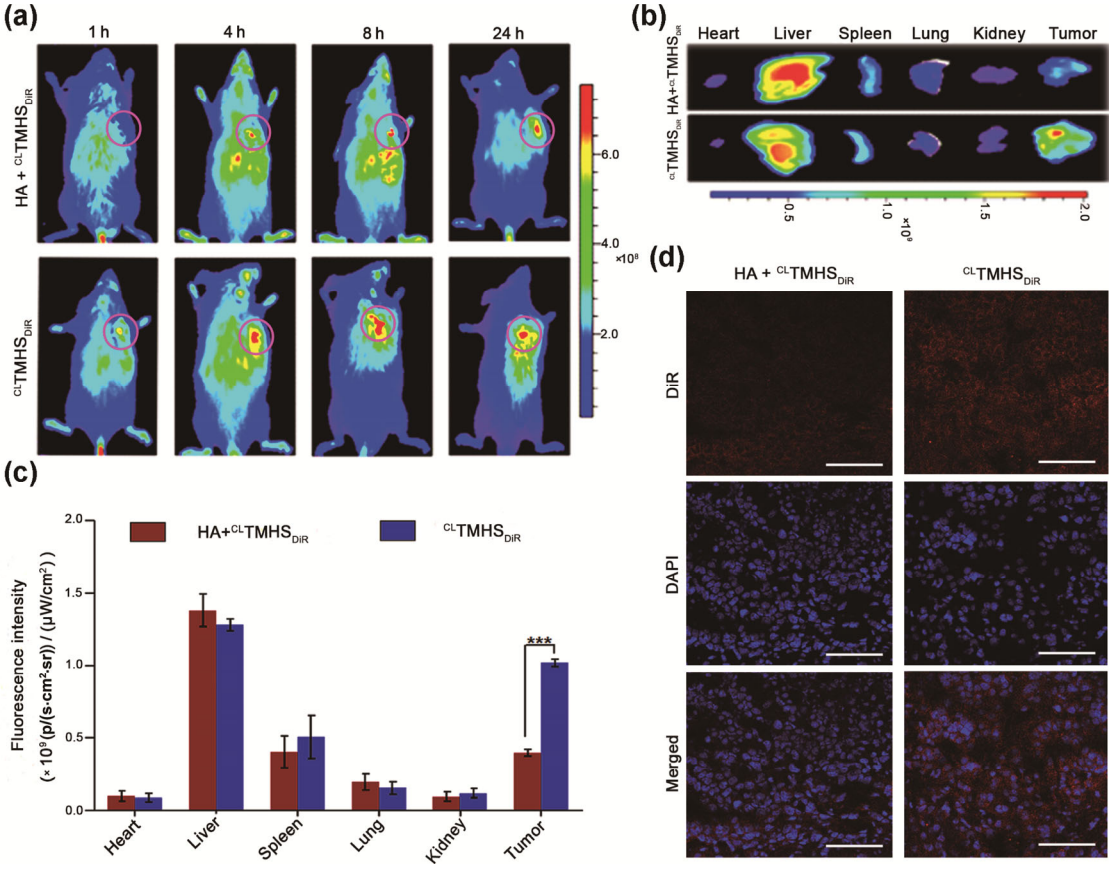

Figure 6 (a) *In vivo* imaging of tumor-bearing nude mice after injection of $^{CL}TMHS_{DiR}$ gel-micelles with or without pre-treatment of HA at 1, 4, 8, and 24 h. (b) Fluorescence imaging of major organs collected at 24 h post-injection. (c) Quantification of mean fluorescence intensity in main organs at 24 h post-injection. (d) CLSM images of HepG2 tumor sections at 24 h after injection of $^{CL}TMHS_{DiR}$ micelles with or without pre-administration of HA (Nuclei were stained with DAPI (blue color), scale bar = 100 μm). Data are presented as mean ± SD, $n = 4$, $^{***}p < 0.001$.

the fluorescence intensity of harvested tumor tissue from ^{CL}TMHS$_{DiR}$ group was 2.54-fold higher than that of HA-pretreated group (Figs. 6(b) and 6(c)), and 11.49-, 2.01-, 6.58-, and 8.50-fold of that at heart, spleen, lung, and kidney respectively. The higher fluorescence biodistribution in hepatic tissues appears reasonable given that liver sinusoidal endothelial cells expressed specific receptors of HA according to previous reports [42]. These results showed that TMHS gel-micelles possessed a remarkable targeting ability as well as the potential to reduce side effects of chemotherapeutics toward major organs. The frozen tissue slices of excised tumors were further analyzed using CLSM. The preferential accumulation of ^{CL}TMHS$_{DiR}$ micelles at the tumor site was in accordance with *in vivo* imaging analysis (Fig. 6(d)), which provided conclusive evidence that the cross-linked TMHS micelles gave high tumor-specific drug delivery efficiency owing to synergistic effects of EPR and CD44 receptor mediated cell internalization.

3.10 *In vivo* antitumor efficacy

To demonstrate the feasibility of TMHS conjugates for oncotherapy application *in vivo*, the anticancer activity of ^{CL}TMHS$_{PTX}$ gel-micelles was estimated with HepG2 tumor xenograft models. According to Fig. 7(a), the tumor volumes of saline group rapidly increased up to 800 mm^3 at day 12, more than 7 times larger than the initial. Taxol® (free-PTX) group demonstrated a modest reduction of 12.15% in tumor volume compared to control group. Whereas, the other groups including ^{NCL}MHS$_{PTX}$, ^{CL}MHS$_{PTX}$, and ^{CL}TMHS$_{PTX}$ group generated a noticeably higher inhibition against tumor growth than Taxol®, with noteworthy tumor volume decreases of 26.21%, 27.23%, and 60.63%, respectively. The results could be mainly attributed to the EPR effects of the nanoparticles in combination with active targeting. Notably, the ^{CL}TMHS$_{PTX}$ group demonstrated an enhanced antineoplastic activity compared to those of ^{NCL}MHS$_{PTX}$ and ^{CL}MHS$_{PTX}$ group, further confirming the enhanced antitumor effect by pH-activated flexible PTX release without any body weight variations (Fig. 7(b)). For comparison, noticeable body weight loss was observed in Taxol® group, mostly resulting from nonselective biodistribution and dose-dependent toxicity of Cremophor EL and ethanol in Taxol® preparation. The tumor tissues

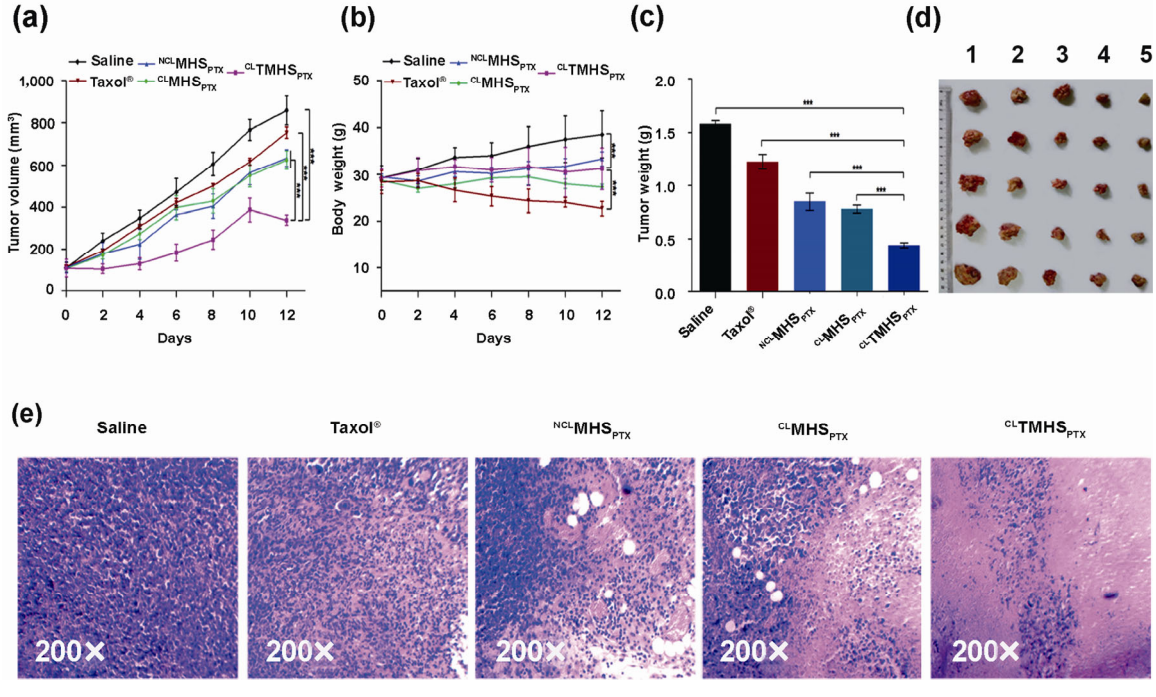

Figure 7 *In vivo* antitumor efficacy in HepG2 tumor-bearing nude mice. Tumor growth curve (a) and body weight changes (b) after treatment with different preparations (n = 5). (c) Tumor weight variation of study groups (n = 5). (d) Images of tumors excised from mice treated with saline (1), Taxol® (2), MHS$_{PTX}$ (3), ^{CL}MHS$_{PTX}$ (4), and ^{CL}TMHS$_{PTX}$ (5) (n = 5). (e) Representative images of H&E stained tumor sections at the conclusion of the study (n = 3). ***p < 0.001.

were collected for accurate weighing after sacrifice of the mice (Figs. 7(c) and 7(d)). $^{CL}TMHS_{PTX}$ group demonstrated the highest tumor weight inhibition capacity of 72.06%, which increased by 1.46-, 1.57-, and 3.25-fold compared to $^{CL}MHS_{PTX}$, $^{NCL}MHS_{PTX}$, and Taxol® group, respectively. Moreover, the prominent capability of $^{CL}TMHS_{PTX}$ gel-micelles on tumor inhibition was also validated by the pathological examination of the H&E staining (Fig. 7(e)). Tumor tissue section images showed greatest degree of cancer cell suppression after the administration of $^{CL}TMHS_{PTX}$ gel-micelles. Overall, stimuli-responsive $^{CL}TMHS_{PTX}$ gel-micelles provided flexible modulation of drug release, and attained the goal of breaking biological and physiological barriers and maximizing antineoplastic efficacy *in vivo*.

3.11 Safety profiles

Biosafety of PTX-loaded TMHS micelles is of key importance in the assessment of the drug delivery platform. Therefore, a hemolytic assay was performed to investigate nanoparticle biocompatibility with RBC membranes for intravenous administration (Fig. 8(a)). Groups treated with Cremophor EL and ethanol and Taxol® induced conspicuous hemolysis at increasing concentrations, reaching 23.21% at 1.60 mg/mL and 48.85% at 0.20 mg/mL. In contrast, $^{CL}TMHS_{Blank}$ and $^{CL}TMHS_{PTX}$ gel-micelles revealed negligible hemolytic effects even at the highest concentrations. These results confirmed that $^{CL}TMHS_{PTX}$ gel-micelles were biocompatible and suitable for intravenous injection. To study whether PTX-loaded micelles would cause any adverse effect during treatment, healthy mice were subjected to the same PTX preparation treatment regimens as mentioned above. The biochemical effects of PTX preparations, such as altered liver and renal function, and microanatomy were then evaluated and compared with those of saline as a control group (Fig. 8(b)). No significant differences were observed between $^{CL}TMHS_{PTX}$ group and control group in the markers of hepatic function, ALT and ALP, nor in the markers of renal function, BUN, and CRE. This indicated negligible hepatotoxicity and nephrotoxicity. However,

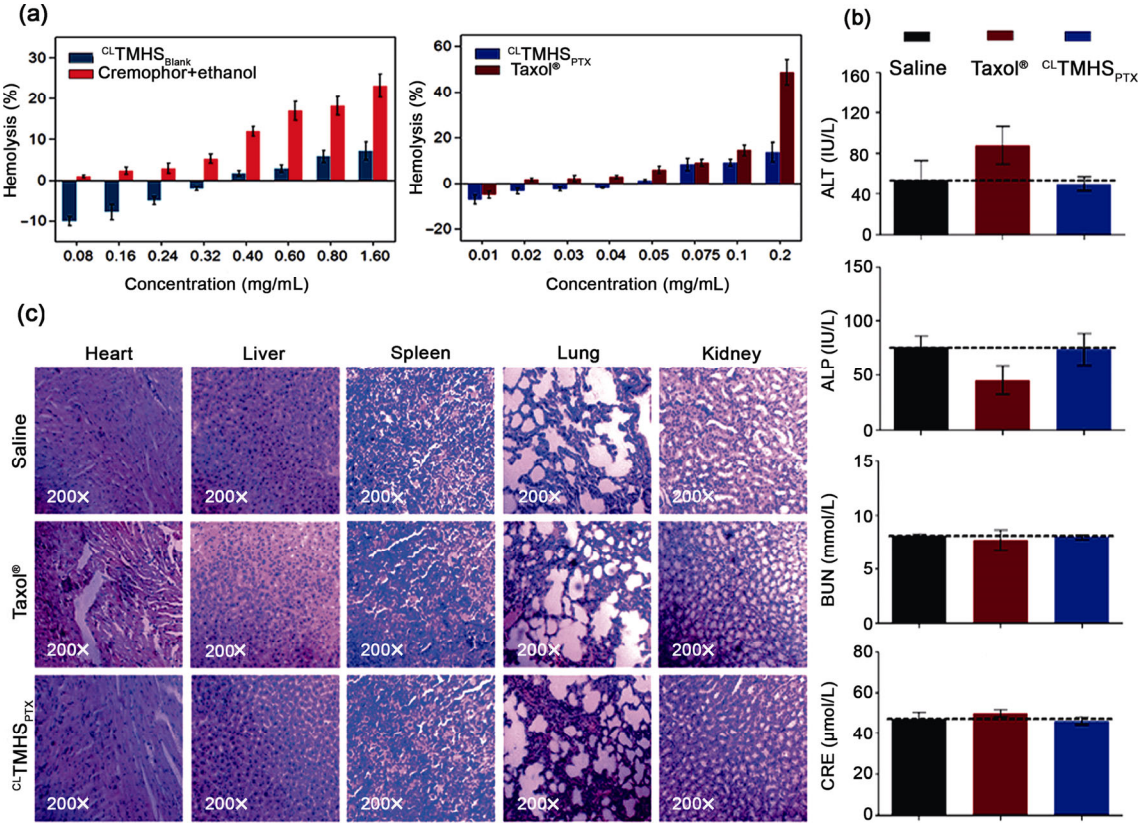

Figure 8 (a) Hemolysis study of carriers and PTX preparations. (b) Evaluation of liver functions (ALT and ALP) and renal functions (BUN and CRE) in healthy mice. (c) Representative images of H&E-stained major tissues. Data are expressed as mean ± SD, $n = 5$.

these parameters did change in the animals treated with Taxol® which might induce acute inflammation in liver and kidney. Moreover, the main organs were collected and examined with H&E staining (Fig. 8(c)). The histological results of Taxol® group demonstrated typical cardiomyopathy characterized by irregularly arranged, dissolved, and broken muscle tissue fibers. Mice in the Taxol® group showed serious liver inflammatory injury, such as liver cell necrosis and moderate inflammatory cell infiltration. Conversely, no pathological abnormalities, degenerations and lesions in main organs were visualized after treatment with $^{CL}TMHS_{PTX}$ or saline; and no changes in the weight ratio of normal organs to body was noticed for $^{CL}TMHS_{PTX}$ treated group (Fig. S3 in the ESM). These results further confirmed that $^{CL}TMHS_{PTX}$ gel-micelles reduced the risk of cardiotoxicity and hepatotoxicity induced by free-PTX, suggesting the safety use of $^{CL}TMHS_{PTX}$ micelles in clinical applications.

4 Conclusions

In this study, a novel HA-based cross-linkable, biodegradable and pH-sensitive amphiphilic TMHS conjugate was successfully synthesized. The conjugate was specifically targeted to CD44-overexpressing cancer cells and was capable of intracellular delivery and flexible modulation of PTX release for maximized antitumor efficacy. Cross-linked TMHS gel-micelles exhibited excellent stability, biocompatibility, and effective drug release *in vitro*. Importantly, TMHS gel-micelles provided an effective pathway for rapid delivery of payloads into the cytosol under acidic condition (pH < 6.5) and in the presence of HAase. Thereby, $^{CL}TMHS_{PTX}$ gel-micelles induced an advanced tumor-targeting ability, enhanced apoptosis, and antitumor efficacy against HepG2 cells *in vitro* and *in vivo*. These findings suggest that the cross-linked TMHS gel-micelles hold great promise for cytosolic flexible release of hydrophobic chemotherapeutics with high biosafety.

Acknowledgements

The authors gratefully acknowledge the financial support from the National Natural Science Foundation of China (Nos. 81501582 and 81573379), the National Key Research and Development Program (No. 2017YFD0501403), and Natural Science Foundation of Jiangsu Province (No. BK20171390). This study was also supported by the National Science and Technology Major Project (Nos. 2017ZX09101001005 and 2017ZX09101001006022), Development Funds for Priority Academic Programs in Jiangsu Higher Education Institutions, and Fostering Plan of University Scientific and Technology Innovation Team of Jiangsu Qing Lan Project (2014).

Electronic Supplementary Material: Supplementary material (plot of the intensity ratio (I_{337}/I_{332}) from pyrene emission spectra versus the logarithm of the concentration (log *C*) of TMHS at pH7.4; changes in particle size and PDI of $^{NCL}TMHS_{PTX}$ and $^{CL}TMHS_{PTX}$ gel-micelles at 4 ˚C within 6 days; the weight ratio of different normal organs to the body) is available in the online version of this article at https://doi.org/10.1007/s12274-018-2012-1.

References

[1] Kuang, H. H.; Ku, S. H.; Kokkoli, E. The design of peptide-amphiphiles as functional ligands for liposomal anticancer drug and gene delivery. *Adv. Drug Deliver. Rev.* **2016**, *110–111*, 80–101.

[2] Jian, C.; Xin, T.; Jie, Z.; Shi, T.; Peng, Z.; Chao, L. Multifunctional cationic polyurethanes designed for non-viral cancer gene therapy. *Acta Biomater.* **2016**, *30*, 155–167.

[3] Sahu, P.; Kashaw, S. K.; Jain, S.; Sau, S.; Iyer, A. K. Assessment of penetration potential of pH responsive double walled biodegradable nanogels coated with eucalyptus oil for the controlled delivery of 5-fluorouracil: *In vitro* and *ex vivo* studies. *J. Control. Release* **2017**, *253*, 122–136.

[4] Stocke, N. A.; Sethi, P.; Jyoti, A.; Chan, R.; Arnold, S. M.; Hilt, J. Z.; Upreti, M. Toxicity evaluation of magnetic hyperthermia induced by remote actuation of magnetic nanoparticles in 3D micrometastasic tumor tissue analogs for triple negative breast cancer. *Biomaterials* **2017**, *120*, 115–125.

[5] Liu, Y.; Wan, G. Y.; Guo, H.; Liu, Y. Y.; Zhou, P.; Wang, H. M.; Wang, D.; Zhang, S. P.; Wang, Y. S.; Zhang, N. A multifunctional nanoparticle system combines sonodynamic therapy and chemotherapy to treat hepatocellular carcinoma. *Nano Res.* **2017**, *10*, 834–855.

[6] Chen, Y.; Li, H. H.; Deng, Y. Y.; Sun, H. F.; Xue, K.; Ci, T. Y. Near-infrared light triggered drug delivery system for higher

efficacy of combined chemo-photothermal treatment. *Acta Biomater.* **2017**, *51*, 374–392.

[7] Cirillo, G.; Spizzirri, U. G.; Curcio, M.; Hampel, S.; Vittorio, O.; Restuccia, D.; Picci, N.; Iemma, F. Carbon nanohybrids as electro-responsive drug delivery systems. *Mini Rev. Med. Chem.* **2016**, *16*, 658–667.

[8] Li, T. S.; Amari, T.; Semba, K.; Yamamoto, T.; Takeoka, S. Construction and evaluation of pH-sensitive immunoliposomes for enhanced delivery of anticancer drug to ErbB2 over-expressing breast cancer cells. *Nanomed. Nanotechnol. Biol. Med.* **2017**, *13*, 1219–1227.

[9] Meng, H.; Wang, M. Y.; Liu, H. Y.; Liu, X. S.; Situ, A.; Wu, B.; Ji, Z. X.; Chang, C. H.; Nel, A. E. Use of a lipid-coated mesoporous silica nanoparticle platform for synergistic gemcitabine and paclitaxel delivery to human pancreatic cancer in mice. *ACS Nano* **2015**, *9*, 3540–3557.

[10] Liao, J. W.; Liu, P. P.; Hou, G. X.; Shao, J. J.; Jing, Y.; Liu, K. Y.; Lu, W. H.; Wen, S. J.; Hu, Y. M.; Peng, H. Regulation of stem-like cancer cells by glutamine through β-catenin pathway mediated by redox signaling. *Mol. Cancer.* **2017**, *16*, 51.

[11] Harnoy, A. J.; Rosenbaum, I.; Tirosh, E.; Ebenstein, Y.; Shaharabani, R.; Beck, R.; Amir, R. J. Enzyme-responsive amphiphilic PEG-dendron hybrids and their assembly into smart micellar nanocarriers. *J. Am. Chem. Soc.* **2014**, *136*, 7531–7534.

[12] Davaa, E.; Lee, J.; Jenjob, R.; Yang, S. G. Mt1-mmp responsive doxorubicin conjugated poly (lactic-*co*-glycolic acid)/poly (styrene-*alt*-maleic anhydride) core/shell microparticles for intrahepatic arterial chemotherapy of hepatic cancer. *ACS Appl. Mater. Interfaces* **2017**, *9*, 71–79.

[13] Chen, W. H.; Luo, G. F.; Lei, Q.; Hong, S.; Qiu, W. X.; Liu, L. H.; Cheng, S. X.; Zhang, X. Z. Overcoming the heat endurance of tumor cells by interfering with the anaerobic glycolysis metabolism for improved photothermal therapy. *ACS Nano* **2017**, *11*, 1419–1431.

[14] Mizrahy, S.; Peer, D. Polysaccharides as building blocks for nanotherapeutics. *Chem. Soc. Rev.* **2012**, *41*, 2623–2640.

[15] Liang, X. L.; Fang, L.; Li, X. D.; Zhang, X.; Wang, F. Activatable near infrared dye conjugated hyaluronic acid based nanoparticles as a targeted theranostic agent for enhanced fluorescence/CT/photoacoustic imaging guided photothermal therapy. *Biomaterials* **2017**, *132*, 72–84.

[16] Cai, Y. P.; López-Ruiz, E.; Wengel, J.; Creemers, L. B.; Howard, K. A. A hyaluronic acid-based hydrogel enabling CD44-mediated chondrocyte binding and gapmer oligonucleotide release for modulation of gene expression in osteoarthritis. *J. Control. Release* **2017**, *253*, 153–159.

[17] Zhou, B.; Weigel, J. A.; Fauss, L.; Weigel, P. H. Identification of the hyaluronan receptor for endocytosis (HARE). *J. Biol. Chem.* **2000**, *275*, 37733–37741.

[18] Yang, C. C.; Li, C.; Zhang, P.; Wu, W.; Jiang, X. Q. Redox responsive hyaluronic acid nanogels for treating rhamm (CD168) over-expressive cancer, both primary and metastatic tumors. *Theranostics* **2017**, *7*, 1719–1734.

[19] Wickens, J. M.; Alsaab, H. O.; Kesharwani, P.; Bhise, K.; Amin, M. C. I. M.; Tekade, R. K.; Gupta, U.; Iyer, A. K. Recent advances in hyaluronic acid-decorated nanocarriers for targeted cancer therapy. *Drug Discov. Today* **2017**, *22*, 665–680.

[20] Jeong, J. Y.; Hong, E. H.; Lee, S. Y.; Lee, J. Y.; Song, J. H.; Ko, S. H.; Shim, J. S.; Choe, S.; Kim, D. D.; Ko, H. J. et al. Boronic acid-tethered amphiphilic hyaluronic acid derivative-based nanoassemblies for tumor targeting and penetration. *Acta Biomater.* **2017**, *53*, 414–426.

[21] Zhu, D. Q.; Wang, H. Y.; Trinh, P.; Heilshorn, S. C.; Yang, F. Elastin-like protein-hyaluronic acid (ELP-HA) hydrogels with decoupled mechanical and biochemical cues for cartilage regeneration. *Biomaterials* **2017**, *127*, 132–140.

[22] Noh, I.; Kim, H. O.; Choi, J.; Choi, Y.; Dong, K. L.; Huh, Y. M.; Haam, S. Co-delivery of paclitaxel and gemcitabine via CD44-targeting nanocarriers as a prodrug with synergistic antitumor activity against human biliary cancer. *Biomaterials* **2015**, *53*, 763–774.

[23] Han, J.; Park, W.; Park, S.; Na, K. Photosensitizer-conjugated hyaluronic acid-shielded polydopamine nanoparticles for targeted photo-mediated tumor therapy. *ACS Appl. Mater. Interfaces* **2016**, *8*, 7739–7747.

[24] Deng, C.; Jiang, Y. J.; Cheng, R.; Meng, F. H.; Zhong, Z. Y. Biodegradable polymeric micelles for targeted and controlled anticancer drug delivery: Promises, progress and prospects. *Nano Today* **2012**, *7*, 467–480.

[25] Brugués, A. P.; Naveros, B. C.; Calpena Campmany, A. C.; Pastor, P. H.; Saladrigas, R. F.; Lizandra, C. R. Developing cutaneous applications of paromomycin entrapped in stimuli-sensitive block copolymer nanogel dispersions. *Nanomedicine* **2015**, *10*, 227–240.

[26] Tang, L. M.; Zhou, M. L.; Huang, Y.; Zhong, J. J.; Zhou, Z.; Luo, K. Dual-sensitive and biodegradable core-crosslinked HPMA copolymer-doxorubicin conjugate-based nanoparticles for cancer therapy. *Polymer Chem.* **2017**, *8*, 2370–2380.

[27] Zhou, Z. W.; Li, H. P.; Wang, K. K.; Guo, Q.; Li, C. Z.; Jiang, H. L.; Hu, Y. Q.; Oupicky, D.; Sun, M. J. Bioreducible cross-linked hyaluronic acid/calcium phosphate hybrid nanoparticles for specific delivery of siRNA in melanoma tumor therapy. *ACS Appl. Mater. Interfaces* **2017**, *9*, 14576–14589.

[28] Yang, C. C.; Wang, X.; Yao, X. K.; Zhang, Y. J.; Wu, W.; Jiang, X. Q. Hyaluronic acid nanogels with enzyme-sensitive cross-linking group for drug delivery. *J. Control. Release* **2015**, *205*, 206–217.

[29] Guan, X. W.; Li, Y. H.; Jiao, Z. X.; Chen, J.; Guo, Z. P.; Tian, H. Y.; Chen, X. S. A pH-sensitive charge-conversion system for doxorubicin delivery. *Acta Biomater.* **2013**, *9*, 7672–7678.

[30] Wang, D. G.; Wang, T. T.; Liu, J. P.; Yu, H. J.; Shi, J.; Bing, F.; Zhou, F. Y.; Fu, Y. L.; Yin, Q.; Zhang, P. C. et al. Acid-activatable versatile micelleplexes for PD-L1 blockade-enhanced cancer photodynamic immunotherapy. *Nano Lett.* **2016**, *16*, 5503–5513.

[31] Liu, J.; Huang, Y. R.; Kumar, A.; Tan, A.; Jin, S. B.; Mozhi, A.; Liang, X. J. pH-sensitive nano-systems for drug delivery in cancer therapy. *Biotechnol. Adv.* **2014**, *32*, 693–710.

[32] Ma, J.; Kang, K.; Yi, Q. Y.; Zhang, Z. R.; Gu, Z. W. Multiple pH responsive zwitterionic micelles for stealth delivery of anticancer drugs. *RSC Adv.* **2016**, *6*, 64778–64790.

[33] Cong, T. H.; Kang, S. W.; Li, Y.; Kim, B. S.; Lee, D. S. Controlled release of human growth hormone from a biodegradable pH/temperature-sensitive hydrogel system. *Soft Matter* **2011**, *7*, 8984–8990.

[34] Liu, Y. H.; Sun, J.; Cao, W.; Yang, J. H.; Lian, H.; Li, X.; Sun, Y. H.; Wang, Y. J.; Wang, S. L.; He, Z. G. Dual targeting folate-conjugated hyaluronic acid polymeric micelles for paclitaxel delivery. *Int. J. Pharmaceutics* **2011**, *421*, 160–169.

[35] Hachet, E.; Van Den Berghe, H.; Bayma, E.; Block, M.; Auzély-Velty, R. Design of biomimetic cell-interactive substrates using hyaluronic acid hydrogels with tunable mechanical properties. *Biomacromolecules* **2012**, *13*, 1818–1827.

[36] Cui, C.; Xue, Y. N.; Wu, M.; Zhang, Y.; Yu, P.; Liu, L.; Zhuo, R. X.; Huang, S. W. Cellular uptake, intracellular trafficking, and antitumor efficacy of doxorubicin-loaded reduction-sensitive micelles. *Biomaterials* **2013**, *34*, 3858–3869.

[37] Jiang, Y.; Wang, X. Z.; Liu, X.; Lv, W.; Zhang, H. J.; Zhang, M. W.; Li, X. R.; Xin, H. L.; Xu, Q. W. Enhanced antiglioma efficacy of ultrahigh loading capacity paclitaxel prodrug conjugate self-assembled targeted nanoparticles. *ACS Appl. Mater. Interfaces* **2017**, *9*, 211–217.

[38] Cho, E. J.; Sun, B.; Doh, K. O.; Wilson, E. M.; Torregrosa-Allen, S.; Elzey, B. D.; Yeo, Y. Intraperitoneal delivery of platinum with *in-situ* crosslinkable hyaluronic acid gel for local therapy of ovarian cancer. *Biomaterials* **2015**, *37*, 312–319.

[39] Ding, X. F.; Wang, W.; Wang, Y. Z.; Bao, X. L.; Wang, Y.; Wang, C.; Chen, J.; Zhang, F. R.; Zhou, J. P. Versatile reticular polyethylenimine derivative-mediated targeted drug and gene codelivery for tumor therapy. *Mol. Pharmaceutics* **2014**, *11*, 3307–3321.

[40] Han, S.; Liu, Y.; Nie, X.; Xu, Q.; Jiao, F.; Li, W.; Zhao, Y.; Wu, Y.; Chen, C. Efficient delivery of antitumor drug to the nuclei of tumor cells by amphiphilic biodegradable poly(L-aspartic acid-*co*-lactic acid)/DPPE co-polymer nanoparticles. *Small* **2012**, *8*, 1596–1606.

[41] Yue, J.; Liu, S.; Wang, R.; Hu, X. L.; Xie, Z. G.; Huang, Y. B.; Jing, X. B. Transferrin-conjugated micelles: Enhanced accumulation and antitumor effect for transferrin-receptor-overexpressing cancer models. *Mol. Pharmaceutics* **2012**, *9*, 1919–1931.

[42] Raemdonck, K.; Martens, T. F.; Braeckmans, K.; Demeester, J.; De Smedt, S. C. Polysaccharide-based nucleic acid nanoformulations. *Adv. Drug Deliver. Rev.* **2013**, *65*, 1123–1147.